Catalytic Decomposition of Hydrogen Peroxide on Iron Oxide: Kinetics, Mechanism, and Implications

ARTICLE *in* ENVIRONMENTAL SCIENCE AND TECHNOLOGY · APRIL 1998

Impact Factor: 5.33 · DOI: 10.1021/es970648k

2 AUTHORS, INCLUDING:

Mirat Gurol
Gebze Technical University
46 PUBLICATIONS **1,836** CITATIONS

Environ. Sci. Technol. **1998**, *32,* 1417−1423

Catalytic Decomposition of Hydrogen Peroxide on Iron Oxide: Kinetics, Mechanism, and Implications

SHU-SUNG LIN† AND MIRAT D. GUROL*,‡

Air Pollution Control Division, UCL, ITRI, Hsinchu, Taiwan, and Civil and Environmental Engineering Department, San Diego State University, San Diego, California 92182-1324

This research describes the heterogeneous catalytic reactions of H_2O_2 with granular size goethite (α-FeOOH) particles in aqueous solution under various experimental conditions. This is an important reaction for the environment since both H_2O_2 and iron oxides are common constituents of natural and atmospheric waters. Furthermore, iron oxides function as catalysts in chemical oxidation processes used for treatment of contaminated waters with H_2O_2. The results of this study demonstrated that the decomposition rate of H_2O_2 over goethite surface can be described by the second-order kinetic expression $-d[H_2O_2]/dt = k[FeOOH][H_2O_2]$, where $k = 0.031\ M^{-1}\ s^{-1}$, at pH 7 in the absence of any inorganic or organic chemical species. The apparent reaction rate was dominated by the intrinsic reaction rates on the oxide surfaces rather than the mass transfer rate of H_2O_2 to the surface. The activation energy of the reaction of H_2O_2 with the iron oxide surface was determined to be 32.8 kJ/M. The reaction mechanism for the decomposition of H_2O_2 on goethite surface was proposed on the basis of the fundamental reactions describing the surface complexation chemistry for iron oxide and the interaction of H_2O_2 with the surface sites. The kinetic model, which was developed according to the proposed mechanism, was found to be similar to the classical Langmuir−Hinshelwood rate model. The model was calibrated and verified successfully. For low concentrations of H_2O_2, the Langmuir−Hinshelwood model is reduced to the observed second-order kinetic expression.

Introduction

Decomposition of aqueous hydrogen peroxide (H_2O_2) over heterogeneous catalysts, such as the metals Ag, Cu, Fe, Mn, Ni, and Pt and their oxides on supported silica, alumina, and zeolites, has been the subject of earlier investigations (*1*−*7*). The objective of the present paper is to research the kinetics and mechanism of catalytic decomposition of H_2O_2 on goethite (α-FeOOH), a pure crystalline iron oxide, in aqueous medium. Recent observations that various organic contaminants in water or soil can be oxidized by H_2O_2 in the presence of iron oxide minerals (*8*−*15*) provided the motivation for this work. For example, in our recent studies, *n*-chlorobutane (BuCl) was oxidized effectively as a result of rapid decomposition of hydrogen peroxide in the presence of granular goethite particles (*15*). The successful oxidation of BuCl, which was used as a probe for hydroxyl radical (•OH), indicates the formation of •OH as an intermediate of H_2O_2 decomposition. These results will be presented in a future paper. Furthermore, H_2O_2 and iron oxides are common constituents of natural and atmospheric waters (*16*, *17*). Hence, the study of the reactions of H_2O_2 with iron oxides can lead to a better understanding of the fate of H_2O_2 and the extent of the oxidation reactions in the environment.

This study has focused on goethite since it was found to be the most reactive with H_2O_2 among the crystalline iron oxides tested (*18*). Goethite, which has a very low solubility in water, is also the most abundant crystalline iron oxide mineral in nature (*19, 20*).

Experimental Methods

In this study, the experiments were conducted in a batch reactor that was stirred at a speed to provide complete mixing for uniform distribution and full suspension of iron oxide particles. Complete mixing was assured by estimating the segregation number for hydrogen peroxide solution as 3 orders of magnitude smaller than the minimum number required for the fluid to be considered a "microfluid", according to Levenspiel (*21*). Off-bottom suspension of the oxide particles was provided according to the Zwietering correlation estimated for the mixing conditions applied (*22*).

The pH was adjusted by using solutions of NaOH and $HClO_4$, and the pH variation during the reaction was $<\pm 0.1$ pH unit. The samples taken at various time intervals were filtered through a Whatman No. 1 filter paper (11 μm) to separate the iron oxide particles from the solution. The filtrate was then analyzed for pH and the concentrations of H_2O_2 and total dissolved iron.

The granular goethite was purchased from Aldrich Chemical Co. with a size range of ∼0.2−0.6 mm (30−80 mesh). These particles were produced by using a proprietary material to bind the colloidal goethite particles. The surface of goethite examined by scanning electron microscopy revealed a large number of external pores. The surface area was measured by a N_2 gas BET surface area analyzer as 120 m^2/g. This is equivalent to the external surface provided by colloidal particles of 0.015 μm. The density of granular goethite was ∼3.37 g/cm^3. The concentration of the replaceable surface hydroxyl groups of the goethite was determined to be 5×10^{-4} mol/g by measurement of the amount of fluoride adsorption on the surface (*23*). Surface charge and surface acidity of the goethite particles were measured by acid−base titration according to the method of Stumm and Morgan (*20*). The intrinsic acidity constants of the surface, pK_{a1}^{int} and pK_{a2}^{int}, were determined as 6.2 and 9.2, respectively. Hence, the pH of zero point of charge, pH_{zpc}, was estimated as 7.7, which is close to 7.8, the value reported in the literature (*20*).

H_2O_2 concentration was measured according to the permanganate titration method that has a detection limit of 1×10^{-4} M of H_2O_2. Concentration of dissolved ferrous iron was determined spectrophotometrically by the phenanthroline method with a detection limit of 1.8×10^{-6} M. The total dissolved iron was measured by the atomic adsorption method (*24*). All of the suspensions and solutions were prepared with Milli-Q water (Millipore Corp.). The glassware employed in this study was cleaned with 5 N HCl and rinsed several times with Milli-Q water prior to use.

Illumination has been shown earlier to enhance the reduction rates of Fe(III) to Fe(II) on surfaces of iron oxides

* Author to whom correspondence should be addressed [phone: (619) 594-0391; fax: (619) 594-8078; e-mail: mgurol@mail.sdsu.edu].
† Air Pollution Control Division.
‡ Civil and Environmental Engineering Department.

S0013-936X(97)00648-2 CCC: $15.00
Published on Web 04/03/1998

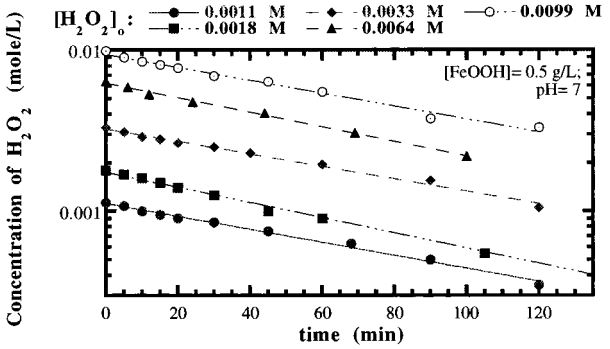

FIGURE 1. First-order fit of H_2O_2 decomposition for different initial concentrations of H_2O_2.

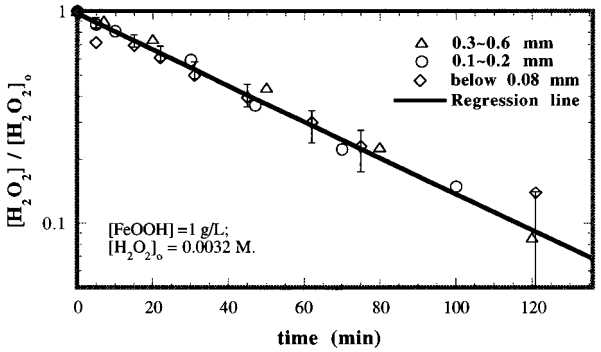

FIGURE 2. First-order fit of H_2O_2 decomposition for different sizes of iron oxide particles.

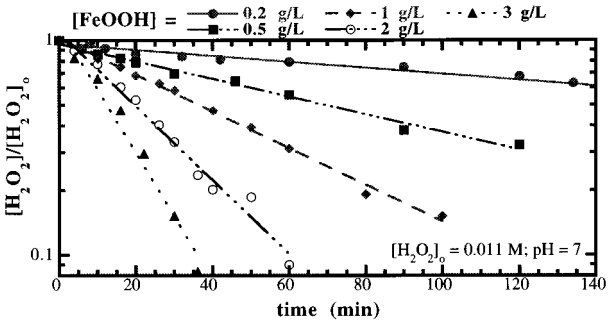

FIGURE 3. First-order fit of H_2O_2 decomposition for different concentrations of iron oxide.

(*25*−*27*). This phenomenon may also cause an enhancement in the decomposition rate of H_2O_2. In the present study, duplicate experiments were conducted under normal laboratory lighting and under darkness (wrapped in foil) to determine whether the laboratory lighting could influence the decomposition of H_2O_2. No effect of illumination was observed under the experimental conditions.

Results and Discussion

Decomposition Kinetics of H_2O_2. The results of the experiments conducted at pH 7 in the presence of 0.5 g/L of FeOOH particles are presented in Figure 1. In the figure, the H_2O_2 concentration is plotted on a log scale as a function of the reaction time for different initial concentrations of H_2O_2, ranging from 0.001 to 0.01 M, which corresponds to the molar H_2O_2/FeOOH ratio of 0.18−1.78. The fit of the data to a straight indicates that the decomposition of H_2O_2 in the presence of FeOOH follows a first-order kinetic rate law

$$-\mathrm{d}[H_2O_2]/\mathrm{d}t = k_{obs}[H_2O_2] \quad (1)$$

and thus

$$\ln([H_2O_2]/[H_2O_2]_0) = -k_{obs}t \quad (2)$$

where k_{obs} is the observed first-order rate constant and $[H_2O_2]$ and $[H_2O_2]_0$ are the concentrations of H_2O_2 in the solution at any time t and time zero, respectively. The lines shown in Figure 1 were fitted to the data by linear regression, which produced correlation coefficients >0.980. The first-order pattern was observed for all of the experiments performed in this study. This is in agreement with the first-order rate kinetics reported earlier for H_2O_2 decomposition on supported iron oxides (*5, 7)* and goethite and ferrihydrite (*28*).

In accordance with eq 2, k_{obs} was found to be independent of the initial concentration of H_2O_2. The mean of the constants (k_{obs}) for five different initial H_2O_2 concentrations was $(9.8 \pm 1.0) \times 10^{-3}$ min^{-1}. Hence, the number of sites on the iron oxide surface available for adsorption of H_2O_2 was not limited under the experimental conditions. This result implies that the rate constant and the kinetic behavior observed in the study can probably be extrapolated to the low H_2O_2 levels observed in natural waters as well.

To understand whether dissolved iron from goethite would contribute significantly to the decomposition of H_2O_2, the dissolved iron concentration was measured after the experiments. The highest total iron concentration measured in the presence of 3 g/L of goethite was ∼0.1 mg/L. The decomposition rate of H_2O_2 at this level of dissolved iron concentration was estimated to be 2 orders of magnitude slower than the rate observed in the presence of iron oxide particles (*19*). Furthermore, the concentration of H_2O_2 was monitored for another 3 h in some of the filtered samples. No significant reduction in H_2O_2 concentration was observed in the absence of goethite particles.

Rate Dependency on Iron Oxide Concentration. To determine the role of iron oxide in the decomposition of hydrogen peroxide, several experiments were carried out with various goethite sizes (0.0001−0.08, 0.1−0.2, and 0.3−0.6 mm) and concentrations (0.2−3 g/L). The pH was 7, and the same initial concentration of 0.011 M H_2O_2 was used in the experiments. The molar H_2O_2/FeOOH ratio varied from 0.33 to 4.89. The experimental observations are presented in Figures 2 and 3 with the logarithm of hydrogen peroxide concentrations plotted as a function of the reaction time. The figures show the experimental data and the fitted regression lines. As depicted in Figure 2, the decomposition rate of H_2O_2 appears to be independent of the goethite particle size. On the other hand, the decomposition rate is directly proportional to the iron oxide concentration (Figure 3). Hence, it can be concluded that the concentration of iron sites, rather than the particle size, is the important factor in these reactions. A similar observation was also reported by Ravikumar and Gurol (*11)* for the decomposition of H_2O_2 on sand particles.

Generally, the external surface area of particles increases with reducing particle size. However, the granular goethite particles used in this study are made up of the colloidal particles the external surfaces of which serve as internal pores for the granular particles. In fact, the BET surface area of the granular particles in the size ranges of 0.3−0.5 and 0.0001−0.08 mm were 120 and 99 m^2/g, respectively, indicating that the particle size did not have a significant effect on the surface area. The large surface area measured for the granular particles is equivalent to the external surface area of the colloidal particles, as reported in the literature. This might explain the observed lack of size effect in the present study.

A plot of the observed first-order rate constants, that is, the slopes of the straight lines in Figure 3, as a function of FeOOH concentration is shown in Figure 4. On the basis of the linear relationship between the rate constants and the

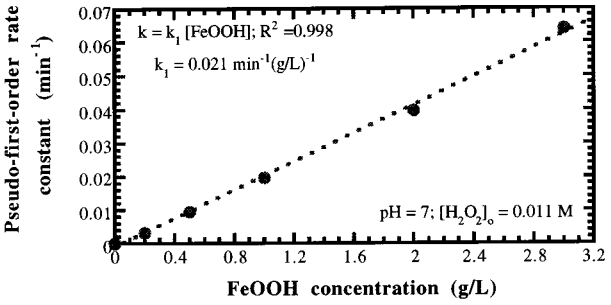

FIGURE 4. First-order rate constant as a function of iron oxide concentration.

concentration of the iron oxide, the rate expression for the H_2O_2 decomposition can now be modified as

$$-d[H_2O_2]/dt = k_1[FeOOH][H_2O_2] \quad (3)$$

where $k_1 = 0.021$ min^{-1}(g/L as FeOOH)$^{-1}$ or 0.032 s^{-1} M^{-1} (as iron) since 1 g/L FeOOH is equivalent to 0.011 M iron. This rate constant can also be expressed on the basis of the average surface area of 110 m^2/g as 3.2×10^{-6} s^{-1} (m^2/L)$^{-1}$. The first-order relationship with respect to the concentrations of H_2O_2 and FeOOH indicates that the rate-determining step in hydrogen peroxide decomposition can be described by

$$\equiv Fe^{III}OH + H_2O_2 \rightarrow \equiv Fe^{II}{-}OH_2 + HO_2^{\bullet} \quad (4)$$

where $\equiv Fe^{III}OH$ represents the iron oxide surface. However, the overall reaction rate will include various steps such as diffusion of chemicals to the surface, surface complex formation (that is, specific adsorption on the reactive sites), actual electron transfer, dissociation of the successor complex (that is, desorption of products), and (re)generation of the reactive sites, as will be elaborated in the following sections.

Diffusion versus Chemical Reaction and Temperature Effect. The apparent rate of a heterogeneous reaction is usually dominated by either the rate of intrinsic chemical reactions on the surface or the rate of diffusion of the solutes to the surface. In this study, the reaction−diffusion modulus (Thiele modulus, ϕ) was estimated according to Levenspiel (*21*) to elucidate the rate-dominating step. ϕ is expressed as the ratio of the reaction rate to the diffusion rate

$$\phi = [k/(D/L^2)]^{0.5} \quad (5)$$

where k is the first-order reaction rate constant (s^{-1}), D is the diffusion coefficient (cm^2/s), and L is the thickness of the stagnant liquid film or the pore length (cm). If ϕ is estimated to be <0.5, the rate of diffusion is concluded to be faster than the reaction rate, but ϕ >5 suggests a strong liquid diffusion resistance.

Since the granular goethite used in this study was quite porous, the mass transfer rate of solutes by diffusion through the liquid film (external mass transfer resistance) and the pore diffusion (internal mass transfer resistance) were considered. The diffusion coefficient of the solutes in liquids is typically $\sim 10^{-5}$ cm^2/s, and the stagnant layer thickness of the liquid film can be estimated by the Film theory as $\sim 10^{-3}$ cm on the basis of a typical mass transfer coefficient of 0.01 cm/s in agitated vessels (*29*). The maximum k measured for the decomposition rate of hydrogen peroxide and the oxidation rate of BuCl at different concentrations of H_2O_2 and FeOOH is $\sim 5 \times 10^{-3}$ s^{-1}. Hence, we can estimate ϕ as 0.02 for external mass transfer. To estimate the rate of internal diffusion, the pore length for spherical porous particles can be taken as equal to one-third of the radius of the particle size (*21*). Hence, the pore length for the granular goethite particles can be estimated as 0.003−0.01 cm. The effective diffusivity of the solutes in the pores generally is $\sim 10^{-6}$ cm^2/s (*21*). Therefore, we can estimate ϕ as 0.07−0.21 for the internal mass transfer. These values of ϕ imply that the average rate of reaction of H_2O_2 on the iron oxide surface is far slower than its diffusion rate to the surface through either the external film or the internal pores. Therefore, the intrinsic reactions on the oxide surface are expected to be the rate-limiting steps for this process. The lack of particle size effect also confirms this conclusion since the rates of internal and external diffusion are generally inversely proportional to the particle size.

TABLE 1. Second-Order Rate Constants for the Reactions of H_2O_2 with Ferric and Ferrous Ions, Supported Iron, Goethite, and Ferrihydrite

catalyst	rate constant (M^{-1} s^{-1})	pH	ref
ferrous ion	0.044	2	*31*
ferric ion	0.024	2	*32*
ferric ion	0.054	2	*33*
ferric ion	0.009−0.09	2.8	*34*
ferric ion	0.002−0.01	2−4	*35*, *36*
Fe_2O_3/Al_2O_3	0.037	12	*5*
Fe_2O_3/Al_2O_3	0.013−0.031	9	*7*
goethite	0.0016	7.7	*28*
ferrihydrite	0.023	7.7	*28*
goethite	0.019−0.067	5−10	this study
goethite	0.032	7	this study

Additional experiments were conducted at temperatures of 6, 25, and 50 °C to determine the activation energy of the reaction of H_2O_2 with the oxide surface. The data were treated on the basis of the Arrhenius equation, and the activation energy of the reaction was determined as 32.8 kJ/mol. This value is higher than the activation energy of the diffusion-controlled reactions, which usually ranges within 10−13 kJ/mol (*20*). Hence, it is confirmed one more time that the apparent reaction rate for this process is dominated by the rate of intrinsic chemical reactions on the oxide surface rather than the rate of mass transfer.

Surface Reactivity. An important question regarding the H_2O_2/FeOOH system is whether the oxidation/reduction reactions on the oxide surface can transform the goethite particles into a less stable and more soluble iron oxide, that is, cause the formation of an amorphous precipitate at the surface of the crystalline phase. Such a mechanism has been proposed by Sulzberger and Laubscher (*25*) for photodissolution of the iron oxides by oxalate. This transformation may lead to a substantial change in the surface characteristics of the mineral, causing a different kinetic behavior and decomposition rate for H_2O_2. This is due to the fact that the surface reactivities of the iron oxides are different for each type of iron oxide (*30*). Furthermore, large amounts of iron dissolution will reduce the concentration of iron oxide and change the mechanism of the reaction from surface based to solution based. However, the experimental results showed that the observed kinetics and rate constants were not affected by various concentrations of H_2O_2, and the dissolved iron concentration was always low (≤0.2 mg/L). In addition, the preliminary experiments conducted in our laboratory by using a continuous flow fixed bed reactor demonstrated that the reactivity of the oxide did not vary over several weeks of operation. Hence, it can be concluded that under the experimental conditions of this study, H_2O_2 did not affect the surface reactivity and the structure of the goethite particles. This was further confirmed by taking pictures of the goethite surface by an electron scanning microscope before and after exposure to H_2O_2. The pictures revealed no significant change in the surface structure (*15*).

Comparison with Other H_2O_2/Fe Systems. In this study, the rate constant for the H_2O_2/FeOOH system at pH 7 was

TABLE 2. Mechanism of Fe^{3+}-Initiated Decomposition of H_2O_2 (*32, 33, 35−40*)

(II.1)	$H_2O_2 + Fe^{3+} \rightarrow Fe^{2+} + H^+ + HO_2^{\bullet}$	$k = 0.002\ M^{-1}\ s^{-1}$	(*34*)
(II.2)	$H_2O_2 + Fe^{2+}/FeOH^+ \rightarrow Fe^{3+} + {}^{\bullet}OH + OH^-/2OH^-$	$k = 76 \pm 1.9 \times 10^5\ M^{-1}s^{-1}$	(*38*)
(II.3)	$^{\bullet}OH + Fe^{2+} \rightarrow Fe^{3+} + OH^-$	$k = 5 \times 10^8\ M^{-1}\ s^{-1}$	(*37*)
(II.4)	$HO_2^{\bullet} + Fe^{3+} \rightarrow Fe^{2+} + O_2 + H^+$	$k = 3.3 \times 10^5\ M^{-1}\ s^{-1}$	(*37*)
(II.5)	$HO_2^{\bullet} + Fe^{2+} \rightarrow Fe^{3+} + HO_2^-$	$k = 1.2 \times 10^6\ M^{-1}s^{-1}$	(*37*)
(II.6)	$^{\bullet}OH + H_2O_2 \rightarrow H_2O + HO_2^{\bullet}$	$k = 2.1 \times 10^9\ M^{-1}\ s^{-1}$	(*39*)
(II.7)	$HO_2^{\bullet} + H_2O_2 \rightarrow H_2O + {}^{\bullet}OH + O_2$	$k = 3.1\ M^{-1}\ s^{-1}$	(*39*)

TABLE 3. Weiss Mechanism Proposed for Decomposition of H_2O_2 on Metal Surfaces (*2*)

$S + H_2O_2 \rightarrow S^+ + OH^- + {}^{\bullet}OH$	(III.1)
$^{\bullet}OH + H_2O_2 \rightarrow H_2O + HO_2^{\bullet}$	(III.2)
$S^+ + O_2^{\bullet -} \rightarrow S + O_2$	(III.3)
$S + HO_2^{\bullet} \rightarrow S^+ + HO_2^-$	(III.4)
$S^+ + HO_2^- \rightarrow S + HO_2^{\bullet}$	(III.5)

determined to be 0.032 $M^{-1}\ s^{-1}$. However, the rate constant varied between 0.019 and 0.067 $M^{-1}\ s^{-1}$ in the pH range of 5−10 (*15*). These constants are listed in Table 1 together with the second-order rate constants reported earlier in the literature for H_2O_2 decomposition in the presence of ferric and ferrous ions, supported iron catalysts, and low-purity goethite and ferrihydrite. The values of the majority of the rate constants reported for different iron catalysts in homogeneous and heterogeneous systems fall in the range of 0.02−0.06 $M^{-1}\ s^{-1}$. Furthermore, the lowest and highest constants in the table differ by only an order of magnitude over a wide pH range. This implies similar kinetic behavior among the systems listed in Table 1.

Reaction Mechanism. The mechanism of the catalytic decomposition of H_2O_2 in the presence of Fe^{2+} has been described in the literature on the basis of the classical Haber−Weiss mechanism (*37*). Here, the initiation reaction involves the oxidation of Fe^{2+} resulting in the formation of hydroxyl radical, as presented in

$$H_2O_2 + Fe^{2+} \rightarrow Fe^{3+} + OH^- + {}^{\bullet}OH \qquad (8)$$

However, this mechanism has been inadequate to describe the reactions of H_2O_2 in solutions of Fe^{3+}, because the initiation reaction in the H_2O_2/Fe^{3+} systems is the reduction of Fe^{3+} to Fe^{2+} by H_2O_2 (*33, 35, 36*). Furthermore, the possible reactions of ferric and ferrous ions with $^{\bullet}OH$ and $HO_2^{\bullet}$ have not been included in the Haber−Weiss mechanism. The mechanism of Fe^3-initiated chain reaction can be summarized by the reaction sequence presented in Table 2 (*32, 33, 35−40*).

In the literature that we had been able to access, the only mechanism that described the decomposition of H_2O_2 over metal oxides was proposed by Kitajima et al. (*5*). These investigators used the Weiss mechanism to explain their kinetic results for decomposition of H_2O_2 on metal oxides, including Fe_2O_3 supported on Al_2O_3. The Weiss mechanism, which had been proposed earlier for metal-catalyzed decomposition of H_2O_2 (*2*), is presented in Table 3 for comparison purposes. Here, S and S^+ represent the uncharged and charged parts of the metal surface. In this mechanism, the principal role of H_2O_2 is the oxidation of the metal surface, resulting in formation of hydroxyl radical by a mechanism similar to the traditional Haber−Weiss mechanism (see reaction 8). However, the initiation reaction in systems involving iron oxides is expected to be the interaction of H_2O_2 with Fe(III) sites on the surface; hence, the Weiss mechanism cannot appropriately describe the reaction mechanism for decomposition of H_2O_2 over surfaces of iron oxides.

Accordingly, the mechanism proposed in this study involves a series of chain reactions similar to the ones described for the Fe^3-initiated decomposition of H_2O_2. As presented in Table 4, the reactions are initiated by the formation of a precursor surface complex of H_2O_2 with the oxide surface, $\equiv Fe^{III}—OH$ (reaction IV.1). $(H_2O_2)_s$ represents the surface species of hydrogen peroxide, which might possess an inner- or an outer-sphere surface coordination. However, the progression of the reaction is expected to be through the inner-sphere formation directly with the surface metal centers. The surface complex may undergo a reversible electron transfer, which can be described as a ground-state electron transfer from ligand-to-metal within a surface complex (reaction IV.2). The electronically excited state can be deactivated through the dissociation of the peroxide radical (dissociation of the successor complex), as shown by reaction IV.3. The peroxide radical is a very active radical that can immediately react with other compounds. Therefore, the reverse of reaction IV.3 may be assumed to be negligible ($k_3 \gg k_{3a}$). It should be noted that reactions IV.1 and IV.2 are unbalanced.

The reduced iron, being a reductant, can react with either H_2O_2 or oxygen, as shown in reactions IV.4 and IV.4a. Surface lattice Fe(II) of goethite particles may be assumed to have similar redox potential and rate constants as $FeOH^+$ in solutions (*25, 41*). The rate constants of $FeOH^+$ with hydrogen peroxide and with oxygen have been determined experimentally as $1.9 \times 10^6\ M^{-1}\ s^{-1}$ (*39*) and 20−40 $M^{-1}\ s^{-1}$ (*42*), respectively. Accordingly, reaction IV.4a is expected to be much slower than reaction IV.4. Furthermore, no significant effect of dissolved oxygen on the decomposition rate of H_2O_2 was observed in our experiments (*15*). Therefore, reaction IV.4a will be ignored for the purpose of developing the kinetic expressions for H_2O_2 decomposition. The peroxide and hydroxyl radicals produced during the reaction may react with Fe(III) and Fe(II) sites on the surface according to reactions IV.6 and IV.7. These free radicals may also react with adsorbed H_2O_2 (reactions IV.8 and IV.9). Finally, radicals may react with each other, terminating the reactions (reactions IV.10 and IV.11). In this part of the study, during which the pH was maintained at 7, H_2O_2 was assumed to react only with $\equiv Fe^{III}—OH$. The protonation equilibria of unoccupied surface groups, that is, the species $\equiv Fe^{III}—OH_2^+$ and $\equiv Fe^{III}—O^-$, and their effects on H_2O_2 decomposition will be presented in a subsequent paper.

Since the peroxide and hydroxyl radicals are quite reactive, it is plausible that they will react with H_2O_2 and other species on the oxide surface before being able to diffuse back to the solution. Nevertheless, the concept of the reaction−diffusion modulus, ϕ, can be used to quantitatively compare the typical reaction and diffusion rates of the radicals The reactions of radicals with other species usually follow second-order kinetics; hence, the rate constant (k) in eq 5 can be modified as

$$k = k_{2nd}[S] \qquad (9)$$

where k_{2nd} is the second-order rate constants and [S] is the surface concentration of the species that the radical reacts with. If it is assumed that $HO_2^{\bullet}$ and $^{\bullet}OH$ will react with the

TABLE 4. Proposed Reaction Mechanism for H_2O_2 Decomposition on Iron Oxide Surface

$$\equiv Fe^{III}\text{—}OH + H_2O_2 \underset{k_{1a}}{\overset{k_1}{\leftrightarrow}} (H_2O_2)_s \quad \text{(IV.1)}$$

$$(H_2O_2)_s \underset{k_{2a}}{\overset{k_2}{\leftrightarrow}} (\equiv Fe^{II}\,{}^{\bullet}O_2H) + H_2O \quad \text{(IV.2)}$$

$$(\equiv Fe^{II}\,{}^{\bullet}O_2H) \underset{k_{3a}}{\overset{k_3}{\leftrightarrow}} \equiv Fe^{II} + HO_2^{\bullet} \quad \text{(IV.3)}$$

$$\equiv Fe^{II} + H_2O_2 \xrightarrow{k_4} \equiv Fe^{III}\text{—}OH + {}^{\bullet}OH + H_2O \quad \text{(IV.4)}$$

$$\equiv Fe^{II} + O_2 \xrightarrow{k_{4a}} \equiv Fe^{III}\text{—}OH + HO_2^{\bullet} \quad \text{(IV.4a)}$$

$$HO_2^{\bullet} \leftrightarrow H^+ + O_2^{\bullet -} \qquad pK_A = 4.8\ (45) \quad \text{(IV.5)}$$

$$\equiv Fe^{III}\text{—}OH + HO_2^{\bullet}/O_2^{\bullet -} \xrightarrow{k_6} \equiv Fe^{II} + H_2O/OH^- + O_2 \quad \text{(IV.6)}$$

$${}^{\bullet}OH + \equiv Fe^{II} \xrightarrow{k_7} \equiv Fe^{III}\text{—}OH \quad \text{(IV.7)}$$

$${}^{\bullet}OH + (H_2O_2)_s \xrightarrow{k_8} \equiv Fe^{III}\text{—}OH + HO_2^{\bullet} + H_2O \quad \text{(IV.8)}$$

$$(H_2O_2)_s + HO_2^{\bullet}/O_2^{\bullet -} \xrightarrow{k_9} \equiv Fe^{III}\text{—}OH + H_2O/OH^- + {}^{\bullet}OH + O_2 \quad \text{(IV.9)}$$

$$HO_2^{\bullet} + HO_2^{\bullet} \xrightarrow{k_{10}} (H_2O_2)_s + O_2 \quad \text{(IV.10)}$$

$${}^{\bullet}OH + HO_2^{\bullet}/O_2^{\bullet -} \xrightarrow{k_{11}} H_2O + O_2\Big) \quad \text{(IV.11)}$$

absorbed surface species at rates similar to those in solutions, the rate constants reported in Table 2 for reaction of $HO_2^{\bullet}$ with Fe^{3+} (reaction II.4) and for reaction of ${}^{\bullet}OH$ with H_2O_2 (reaction II.6) can be used to estimate the value of the Thiele modulus for the radicals. Here, the surface concentration of H_2O_2 was estimated to be $>10^{-5}$ M (*15*), and the goethite concentration used in this study was equivalent to 0.005 M as Fe. Under these conditions, the ϕ for both radicals is estimated to be >5, which indicates that the reaction rates of ${}^{\bullet}OH$ and $HO_2^{\bullet}$ are much faster than their diffusion rates. Hence, we may assume that ${}^{\bullet}OH$ and $HO_2^{\bullet}$ will be completely consumed on the surface prior to diffusing to the solution. Thus, the reactions of ${}^{\bullet}OH$ and $HO_2^{\bullet}$ with solutes in the solution phase are expected to be negligible under the given conditions.

Reaction Kinetics. According to the reaction mechanism described by reactions VI.1—VI.10, the decomposition rate of H_2O_2, r_H, can be presented by the following:

$$-r_H = -d[H_2O_2]/dt = k_1[\equiv Fe^{III}\text{—}OH][H_2O_2] - k_{1a}[(H_2O_2)_s] + k_4[\equiv Fe^{II}][H_2O_2] \quad (10)$$

The steady-state surface concentration of H_2O_2 can be expressed on the basis of reactions VI.1 and VI.2 as

$$[(H_2O_2)_s] = \frac{k_1[\equiv Fe^{III}\text{—}OH]\,[H_2O_2] + k_{2a}[(\equiv Fe^{II}\,{}^{\bullet}O_2H)]}{k_{1a} + k_2} \quad (11)$$

Assuming steady-state conditions for $(\equiv Fe^{II}\,{}^{\bullet}O_2H)$ yields

$$[(\equiv Fe^{II}\,{}^{\bullet}O_2H)] = k_2[(H_2O_2)_s]/(k_3 + k_{2a}) \quad (12)$$

When eq 12 is substituted in eq 11, the following expression is obtained:

$$[(H_2O_2)_s] = \frac{k_1(k_3 + k_{2a})[\equiv Fe^{III}\text{—}OH][H_2O_2]}{k_3(k_{1a} + k_2) + k_{1a}k_{2a}} \quad (13)$$

Assuming steady-state conditions for $(\equiv Fe^{II})]$ yields

$$[(\equiv Fe^{II})] = k_3k_2[(H_2O_2)_s]/\{k_4(k_3 + k_{2a})[H_2O_2]\} \quad (14)$$

Substitution of eqs 13 and 14 in eq 10 will yield the following equation for H_2O_2 decomposition:

$$-\frac{d[H_2O_2]}{dt} = \frac{2k_1k_2k_3[\equiv Fe^{III}\text{—}OH][H_2O_2]}{k_3(k_{1a} + k_2) + k_{1a}k_{2a}} \quad (15)$$

A mass balance equation for the oxide surface sites can be presented as

$$[FeOOH] = [\equiv Fe^{III}\text{—}OH] + [(H_2O_2)_s] + [(\equiv Fe^{II}\,{}^{\bullet}O_2H)] + [\equiv Fe^{II}] \quad (16)$$

where [FeOOH] is the total concentration of the surface sites. Since $\equiv Fe^{II}$ is expected to be oxidized rapidly by H_2O_2 and $\equiv Fe^{II}\,{}^{\bullet}O_2H$ is only a transitional state for the site, the concentrations of the species $(\equiv Fe^{II}\,{}^{\bullet}O_2H)$ and $(\equiv Fe^{II})$ are expected to be very low. Hence, eq 16 can be modified as

$$[\equiv Fe^{III}\text{—}OH] = [FeOOH] - [(H_2O_2)_s] \quad (17)$$

Substitution of eqs 17 and 14 in eq 15 leads to

$$-r_H = -\frac{d[H_2O_2]}{dt} = \frac{k[FeOOH][H_2O_2]}{1 + K_H[H_2O_2]} \quad (18)$$

where $K_H = \{k_1(k_3 + k_{2a})/k'\}$, $k = 2k_1k_2k_3/k'$, and $k' = k_3(k_{1a} + k_2) + k_{1a}k_{2a}$.

According to eq 18, which resembles the classic Langmuir—Hinshelwood rate expression, the rate of H_2O_2 decomposition is first order with respect to the concentration of surface sites on iron oxide. K_H and k represent the binding and rate constants, respectively (*43*). It should be noted that the Langmuir—Hinshelwood kinetic equation has been used empirically to describe many heterogeneous catalytic surface reactions, for example, photocatalytic TiO_2 oxidation of organic compounds (*43*) and reductive dissolution of iron oxide (*44*). However, in the present study, we have been successful in describing this surface phenomenon by using elementary reaction steps that led to the derivation of the Langmuir—Hinshelwood expression.

At constant catalyst concentration, the applicability of eq 18 to the data can be tested by plotting the inverse initial rate (r_{Hi}) versus inverse initial concentration, $[H_2O_2]_0$

$$\frac{[\text{FeOOH}]}{r_{\text{Hi}}} = \frac{K_{\text{H}}}{k} + \frac{1}{k}\frac{1}{[\text{H}_2\text{O}_2]_0} \tag{19}$$

which requires both a positive slope $(k)^{-1}$ and an intercept, (K_{H}/k). Additionally, the proposed kinetic model presented by eq 18 can be calibrated by comparing the experimental observations to the numerical solutions of the model, which were obtained by the fourth-order Runge−Kutta method.

The proposed kinetic model can be reduced, respectively, to zero-order and first-order expressions with respect to $[H_2O_2]$ for the different values of K_{H} $[H_2O_2]$:

case I, $K_{\text{H}}[H_2O_2] \ll 1$

$$-r_{\text{H}} = k[\text{H}_2\text{O}_2][\text{FeOOH}] \tag{20}$$

case II, $K_{\text{H}}[H_2O_2] \gg 1$

$$-r_{\text{H}} = (k/K_{\text{H}})[\text{FeOOH}] \tag{21}$$

Model Calibration. To test whether the proposed kinetic model presented by eq 18 was applicable, the data generated experimentally for various concentrations of H_2O_2 and 0.5 g/L of FeOOH at pH 7 were replotted in Figure 5 according to eq 19. It is clear from the figure that the reciprocal of the rate is directly proportional to the reciprocal of the initial H_2O_2 concentration (R^2 value of 0.990). From the intercept and the slope of the regression line, the reaction rate constant (k) is estimated as 1.84 M^{-1} min^{-1}, or 0.031 M^{-1} s^{-1}, at pH 7. This result is consistent with the experimental observations presented in Table 1 for pH 7. The binding constant (K_{H}) is estimated as 0.280 M^{-1}, which is a very low number. Therefore, when the $[H_2O_2]$ is <1 M (34 000 mg/L), K_{H} $[H_2O_2]$ will be <1, and the proposed model will be reduced to an expression that is first order with respect to $[H_2O_2]$ and [FeOOH], as presented by eq 20.

Model Verification. For the verification of the kinetic model, several additional experiments were conducted at pH 7 with 0.01 M H_2O_2. The results are presented in Figure 6, in which the normalized concentration of H_2O_2 was plotted as a function of time. The predictions of the model were made on the basis of eq 18 or 20 with $k = 0.031$ M^{-1} s^{-1} and $K_{\text{H}} = 0.280$ M^{-1}. The experimental data are represented by the symbols, and model predictions are presented by the solid and dashed lines. The fit of the model to the data was found to be extremely good on the basis of calculation of relative error, which is defined as the absolute value of the difference between the predicted and observed values divided by the predicted values. The average relative error was ≈3.8%, which is less than the 10% experimental error involved in the measurement of H_2O_2, as represented by the bars in the figure. Hence, it can be concluded that the reaction behavior of H_2O_2 on the surface of goethite can be very well described by the Langmuir−Hinshelwood model, which is also consistent with the postulated reaction mechanism. Table 5 presents the proposed reaction mechanism simplified on the basis of model verification.

Environmental Relevance

The results of this study provide insight to the mechanism of chemical oxidation reactions achieved when organic compounds are brought into contact with aqueous solutions of H_2O_2 in the presence of iron oxide minerals for treatment purposes. Furthermore, the experimental evidence implies that the goethite particles may play an important role in the fate of H_2O_2 in surface and seawaters. Sunlight or direct mediation by aquatic Fe (II and III) and other metal ions does not seem to be needed for the reactions to take place. Furthermore, the decomposition of H_2O_2 can lead to the generation of hydroxyl radical that may eventually lead to an important pathway for oxidation/reduction of organic compounds in natural and atmospheric waters. The experiments in this study were conducted with relatively high concentrations of H_2O_2 in the range of 1−10 mM, yet the iron oxide surface was still far from saturation. Furthermore, the kinetic expression obtained on the basis of the observations was validated by the kinetic model derived from a mechanism consisting of fundamental and elemental reaction steps. Therefore, it is quite likely that the kinetic results of this study could be extrapolated to the conditions in the natural environment, where H_2O_2 concentration is typically 100−1000 times lower. It should also be noted that even when H_2O_2 concentration is as low as 1×10^{-3} mM, the oxidation rate of ferrous sites by H_2O_2 (reaction IV.4) is expected to be ~700 times faster than the oxidation rate of ferrous sites by oxygen (reaction IV.4a).

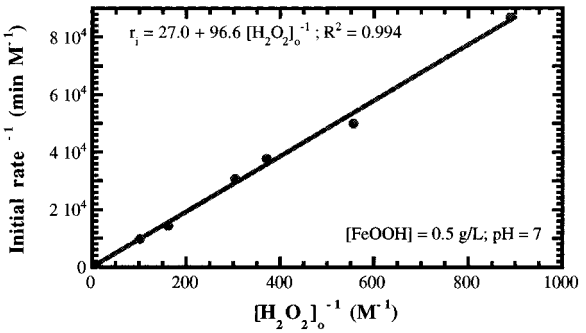

FIGURE 5. Reciprocal of initial rates versus reciprocal of initial concentrations of H_2O_2.

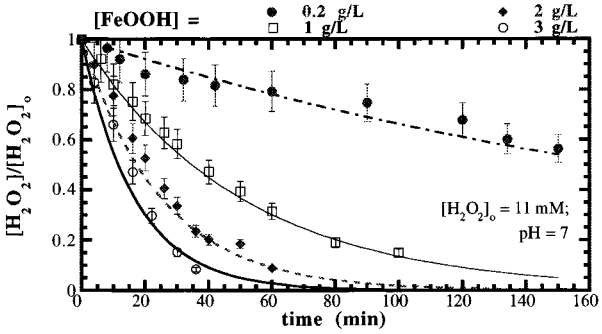

FIGURE 6. Model verification for H_2O_2 decomposition at different iron oxide concentrations.

TABLE 5. Simplified Reaction Mechanism for H_2O_2 Decomposition on Iron Oxide Surface

$\equiv Fe^{III}—OH + H_2O_2 \underset{k_{1a}}{\overset{k_1}{\rightleftarrows}} (H_2O_2)_s$	(V.1)
$(H_2O_2)_s \xrightarrow{k_2} \equiv Fe^{II} + H_2O + HO_2^{\bullet}$	(V.2)
$\equiv Fe^{II} + H_2O_2 \xrightarrow{k_3} \equiv Fe^{III}—OH + {}^{\bullet}OH$	(V.3)
$HO_2^{\bullet} \leftrightarrow H^+ + O_2^{\bullet -}$	(V.4)
$\equiv Fe^{III}—OH + HO_2^{\bullet}/O_2^{\bullet -} \xrightarrow{k_5} \equiv Fe^{II} + H_2O/OH^- + O_2$	(V.5)

Acknowledgments

The financial support provided by the U.S. National Science Foundation, Environmental Engineering Program directed by Dr. Edward Bryan under Agreement BES-9407724, is greatly appreciated. The authors were, respectively, a graduate student and a professor at the time of this study at Drexel

University, School of Environmental Engineering, Science and Policy, Philadelphia, PA.

Literature Cited

(1) Weiss, J. *Trans. Faraday Soc.* **1935**, *31*, 1547.
(2) Weiss, J. *Adv. Catal.* **1952**, *4*, 343.
(3) Roy, C. B. *J. Catal.* **1968**, *12*, 129.
(4) Ono, Y.; Matsumura, T.; Kitajima, N.; Fukuzumi, S.-I. *J. Phys. Chem.* **1977**, *81*, 1307.
(5) Kitajima, N.; Fukuzumi, S.-I.; Ono, Y. *J. Phys. Chem.* **1978**, *82*, 1505.
(6) McKee, D. W. *J. Catal.* **1969**, *14*, 355.
(7) Abbot, J.; Brown, D. G. *Int. J. Chem. Kinet.* **1990**, *22*, 963.
(8) Dore, M. *Water Res.* **1990**, *24*, 973.
(9) Tyre, B. W.; Watts, R. J.; Miller, G. C. *J. Environ. Qual.* **1991**, *20*, 832.
(10) Watts, R. J.; Udell, M. D.; Monsen, R. M. *Water Environ. Res.* **1993**, *65* (7), 839.
(11) Ravikumar, J. X.; Gurol, M. D. *Environ. Sci. Technol.* **1994**, *28*, 394.
(12) Gates, D. D.; Siegrist, R. L. *J. Environ. Eng.* **1995**, Sept, 639−644.
(13) Lin, S. S.; Gurol, M. D. In *Proceedings of 27th Mid-Atlantic Industrial Waste Conference*, Bethlehem, PA; Technomic: Lancaster, PA, 1995; p 352.
(14) Miller, C. M.; Valentine, R. L. *Water Res.* **1996**, *29* (10), 2353.
(15) Lin, S.-S. Ph.D. Dissertation, Drexel University, Philadelphia, PA, 1997.
(16) Moffett, J. D.; Zika, R. G. *Environ. Sci. Technol.*, **1987**, 21, 804.
(17) Cunningham, K. M.; Goldberg, M. C.; Winer, E. R. *Environ. Sci. Technol.* **1988**, *22*, 1090.
(18) Gurol, M. D.; Lin, S. S.; Bhat, N.; Lin, S. Presented at the Advanced Chemical Oxidation Conference, San Francisco, CA, 1997.
(19) Bolt, G. H.; van Riemdijk, W. H. In *Aquatic Surface Chemistry*; Stumm, W., Ed.; Wiley-Interscience: New York, 1987; p 127.
(20) Stumm, W.; Morgan, J. J. *Aquatic Chemistry*, 3rd ed.; Wiley-Interscience: New York, 1996.
(21) Levenspiel, O. *Chemical Engineering Reaction*; Wiley-Eastern Limited: New York, 1972.
(22) Tatterson, G. B. *Scale-up and Design of Industrial Mixing Processes*; McGraw-Hill: New York, 1994; pp 134−145.
(23) Sigg, L.; Stumm, W. *Colloids Surf.* **1980**, *2*, 101−117.
(24) Standard Methods for the Examination of Water and Wastewater; APHA, AWWA, WEF: Washington, DC, 1992.
(25) Sulzberger, B.; Laubscher, H. *Mar. Chem.* **1995**, *50*, 103−113.
(26) Pehkonen, S. O.; Sieferet, R. L.; Webb, S.; Hoffmann, M. R. *Environ. Sci. Technol.* **1993**, *27*, 2056−2062.
(27) Sieffert, C.; Sulzberger, B. *Langmuir* **1991**, 7, 1627−1634.
(28) Wang, A. H.; Valentine, R. L. In *Proceedings of the Third International Symposium on Chemical Oxidation: Technology for the Nineties*, Nashville, TN; Technomic: Lancaster, PA, 1993; p 74.
(29) Sherwood, T. K.; Pigford, R. L.; Wilke, C. *Mass Transfer*; McGraw-Hill: New York, 1975; p 222.
(30) Kung, K.-H.; McBride, M. B. *Soil Sci. Soc. Am. J.* **1989**, *53*, 1673.
(31) Martin, L. R.; Easton, M.; Foster, J. W.; Hill, M. W. *Atmos. Environ.* **1989**, *23*, 563.
(32) Eary, L. E. *Metall. Trans. B.* **1986**, *16B*, 181.
(33) Barb, W. G.; Baxendale, J. H.; George, D.; and Hargrave, K. R. *Faraday Soc. Trans.* **1959**, *47*, 591.
(34) Pignatello, J. J. *Environ. Sci. Technol.* **1992**, *26*, 944.
(35) Walling, C.; Weil T. *Int. J. Chem. Kinet.* **1974**, *5*, 507.
(36) Walling, C.; Cleary, M. *Int. J. Chem. Kinet.* 1**977**, *9*, 595.
(37) Haber, F.; Weiss, J. *Proc. R. Soc. Ser.* **1934**, *T27*, 332−351.
(38) Rush, J. D.; Bielski, B. H. *J. Phys. Chem.* **1985**, *89*, 5062.
(39) Moffett, J. D.; Zika, R. G. *Environ. Sci. Technol.* **1987**, *21*, 804.
(40) Buxton, G. V.; Greenstock, C. L.; Helman, W. P.; Ross, A. B. *J. Phys. Chem. Ref. Data* **1988**, *17*, 5T1.
(41) Xue, Y.; Traina, S. J. *Environ. Sci. Technol.* **1996**, *30*, 1975−1981.
(42) Singer, P. C.; Stumm, W. *Science* **1970**, *167*, 1121−1123.
(43) Ollis, D. F.; Serpone, N.; Pelizzetti, E. In *Photocatalysis Fundamentals and Applications*; Serpone, N., Pelizzetti, E., Eds.; Wiley: New York, 1989; pp 603−638.
(44) Stumm, W.; Sulzberger, B. *Geochim. Cosmochim. Acta* **1992**, *56*, 3233.
(45) Behar, D.; Czapski, G.; Rabani, J.; Dorfman, L. M.; Schwarz, H. A. *J. Phys. Chem.* **1970**, *74*, 3209−3211.

Received for review July 24, 1997. Revised manuscript received January 27, 1998. Accepted February 17, 1998.

ES970648K